Supplementary Materials: "Self-starting soliton-comb regimes in $\chi^{(2)}$ microresonators"

Sergey Smirnov[1] , Evgeni Podivilov[2] and Boris Sturman[2]

1. Whispering gallery modes

Optical whispering gallery modes (WGMs) exist is any axially symmetric body (sphere, spheroid, toroid, etc.) made of a transparent material [17,24-26]. Owing to the azimuth symmetry, all components of the light fields are proportional to $\exp(im\varphi)$, where φ is the azimuth angle and m is the azimuth number taking integer values. Typically, the vacuum wavelength $\lambda = 2\pi c/\omega$ is much smaller than the major radius R, the azimuth number $m \gg 1$, and the light fields are strongly localized near the rim. Exact WGM solutions to the Maxwell equations with true boundary conditions are available only for the spherical case [24,25]. In other practically important cases, including the $\chi^{(2)}$ case, approximate solutions, employing smallness of the ratio λ/R, are in use [24,27-30]. While the radiation damping of WGMs is present, it is negligibly small for typical values of the refractive index n and $\lambda \ll R$, such that the modal decay is due to the bulk absorption and roughness of the surface. Typical modal Q-factors are as high as $10^7 - 10^9$, correspondingly, the modal line widths are in the MHz range.

Generally, there are two polarization types of WGMs, and each type is characterized (in addition to m) by two modal numbers – the radial number $q = 1, 2, \ldots$ and the polar number $p = 0, 1, \ldots$. For each polarization type, the modal frequency can be represented as $\omega = k_m c/n$, where $k_m = m/R$ and $n = n(m, q, p)$ is the effective modal refractive index. For $\lambda \ll R$, the modal index is close to its bulk value $n_b(\lambda)$ and $m \simeq 2\pi R n_b/\lambda$. Thus, WGMs can be viewed as quasi-plane waves propagating along the rim with discrete wavevectors k_m and possessing refractive indices slightly dependent on the modal numbers. Within the optical range, the azimuth numbers are $\sim 10^4$. The intermodal distance measured in Hz, $\delta\omega/2\pi = c/2\pi Rn$, is named the free spectral range. It corresponds $\delta\lambda/\lambda = \lambda/2\pi Rn \ll 1$.

The case of uniaxial (birefringent) medium with the optic axis coinciding with the axial one is typical for $\chi^{(2)}$ resonators. Here the modal polarization is either ordinary (o) or extraordinary (e), and the corresponding refractive indices are n_o and n_e. As WGMs are localized near the rim, knowledge of its minor radius r is usually sufficient to calculate $n_{o,e}(m, q, p)$ with a good accuracy. The corresponding relation for the geometric dispersion reads [17,29]

$$\frac{n_b - n}{n_b} \simeq \frac{\zeta_q}{2^{1/3}m^{2/3}} + \frac{(2p+1)\sqrt{R}}{2m\sqrt{r}}, \tag{1}$$

where ζ_q is q-th zero of the Airy function $\mathrm{Ai}(-\zeta)$, such that $\zeta_1 \simeq 2.338$, $\zeta_2 \simeq 4.088$, etc. The right-hand side of Eq. (**??**) represents two first terms of an asymptotic expansion in fractional powers of $1/m$. The higher-order terms of this expansion usually are not necessary for evaluation of $\delta n = n - n_b$. Because of the above link between m and λ, one can easily represent δn as a function of λ. Equation (**??**) is useful for analysis of the effects of geometric dispersion, including the phase matching and minimization of the temporal walk-off. It has to be supplemented by proper empiric Sellmeier equations for $n_b(\lambda)$ [49].
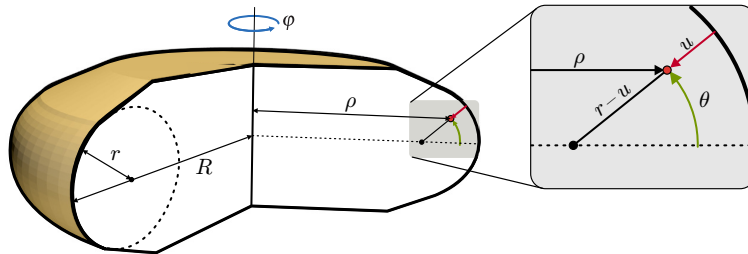

Figure S1. Geometry of the problem; R and r are the major and minor radii of the resonator, while u, θ, and φ are the curvilinear coordinates, and $\rho = \rho(u, \theta)$ is the distance from the observation point (shown by the red dot) to the vertical rotational axis.

In addition to polarization and frequency, each mode can be characterized by the modal function $\Psi_{m,q,p}(\boldsymbol{r}) = \exp(im\varphi)\,\psi_{m,q,p}(\boldsymbol{r}_\perp)$, where $\boldsymbol{r}_\perp$ refers to the transverse cross-section $\varphi = const$. The pre-exponent ensures orthogonality

of two wave functions with different azimuth numbers. The functions $\psi_{m,q,p}(\mathbf{r})$, that can be chosen real, obey the

orthogonality relation

$$\int \psi_{m,q,p}(\mathbf{r}_\perp)\,\psi_{m,q',p'}(\mathbf{r}_\perp)\,d\mathbf{r}_\perp = \delta_{qq'}\delta_{pp'}\,. \tag{2}$$

Obviously, $\psi_{m,q,p}(\mathbf{r}_\perp)$ has the dimension of r^{-1}. The overlap integral $\sigma_{\text{eff}}^{-1/2} = \int \psi_{m_2,q_2,p_2}\psi_{m_1,q_1,p_1}^2\,d\mathbf{r}_\perp$, that occurs in

calculations of elementary $\chi^{(2)}$ processes [31], can be regarded as inverse square root of the interaction cross-section σ_{eff}.

The modal function $\psi_{m,q,p}$ can be calculated within the model of Fig. **??**. More specifically, it is proportional to $U(u)$
and $\Theta(\theta)$, where u is the radial distance to the rim and θ is the azimuth angle measured from equator. Analysis of the
scalar Helmholtz equation for the light field in curvilinear coordinates u, θ results in relations [29]

$$U = U_{m,q} = \text{Ai}\left(\frac{u}{u_m} - \zeta_q\right), \qquad \Theta = \Theta_{m,p} = \exp\left(-\frac{\theta^2}{2\theta_m^2}\right)H_p\left(\frac{\theta}{\theta_m}\right), \tag{3}$$

where $u_m = R/2^{1/3}m^{2/3}$, $\theta_m = (R/r)^{3/4}/m^{1/2}$, and $H_p(x)$ is the Hermitian polynomial of the order p. For $m \gg 1$, both
the modal function is strongly localized in u and θ. Note that $U(0) = 0$, i.e., strongly decaying evanescent fields for $u < 0$
are ignored. More accurate and cumbersome relations are available as well. Equations (**??**) are useful to evaluate modal
overlap integrals entering relations for the nonlinear coupling constants.

2. Impact of geometric dispersion on natural PM and walk-off in LN resonators

Here we use temperature dependent Sellmeier relations of [55] for $n_{\text{o,e}}^b(\lambda)$ relevant to congruent LN crystals doped
with Mg. These crystals are most suitable for manufacturing microresonators. Consider two spectral characteristics
– the phase velocity $V = \omega(k)/k$ and the group velocity $v = d\omega/dk$ – relevant to o and e polarizations. With $n(\lambda)$
known, we have $V = c/n$ and $v = c/(n - \lambda n')$ with $n' = dn/d\lambda$. The velocity differences $V_{12} = V_{\text{o}}(\lambda_1) - V_{\text{e}}(\lambda_1/2)$ and
$v_{12} = v_{\text{o}}(\lambda_1) - v_{\text{e}}(\lambda_1/2)$, where λ_1 is the FH wavelength, characterize the birefringent mismatch and temporal walk-off,
respectively. At $V_{12}(\lambda_1) = 0$ we have a perfect natural (birefringent) phase matching.

Let us neglect first the geometric dispersion. Figures **??**a and **??**b show the dependences $V_{12}(\lambda_1)$ and $v_{12}(\lambda_1)$,
respectively, for two representative values of the temperature T. The ratio V_{12}/c is relatively small. The function $V_{12}(\lambda_1)$
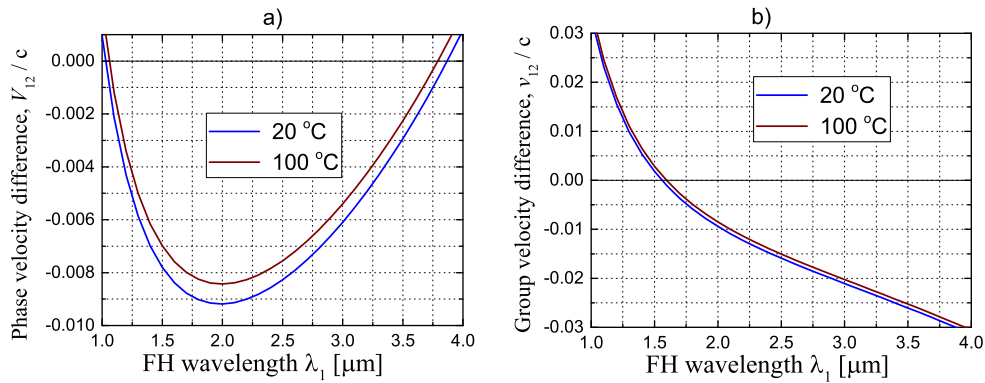

Figure S2. The bulk case: Wavelength dependences of V_{12} (a) and v_{12} (b) for $T = 20$ and $100\,^\circ\text{C}$.

turns to zero for λ_1 slightly exceeding $1\,\mu\text{m}$; the PM point shifts slowly to the right with increasing T. Just this region is
typically used for the natural PM. However, the group velocity difference v_{12} is pretty large in this range. On the other
hand, $v_{12}(\lambda_1)$ turns to zero for $\lambda_1 \simeq 1.58\,\mu\text{m}$; this is far from the point of natural PM. Note also, that the effect of T on
$v_{12}(\lambda_1)$ is relatively weak.

Now we include the effects of geometric dispersion into consideration using Eq. (**??**). Solid lines in Figs. **??**a and **??**b
show dependences of V_{12}/c and v_{12}/c, respectively, on the FH wavelength λ_1 for $T = 20\,^\circ\text{C}$, $R = 1$ mm, $r = 0.25$ mm,
$q_{\text{e}} = 1$, and three representative values of q_{o}. The dashed lines, given for comparison, correspond to the bulk case. We see
that the influence of the geometric dispersion on $V_{12}(\lambda_1)$, subfigure **??**a, is pretty strong: With increasing q_{o} the curves
shift up and left, such that the area between the PM points shrinks. For sufficiently large values of q_{o} and T the phase
matching becomes impossible. As concerned the dependence $v_{12}(\lambda_1)$, it experiences only modest changes: the zero
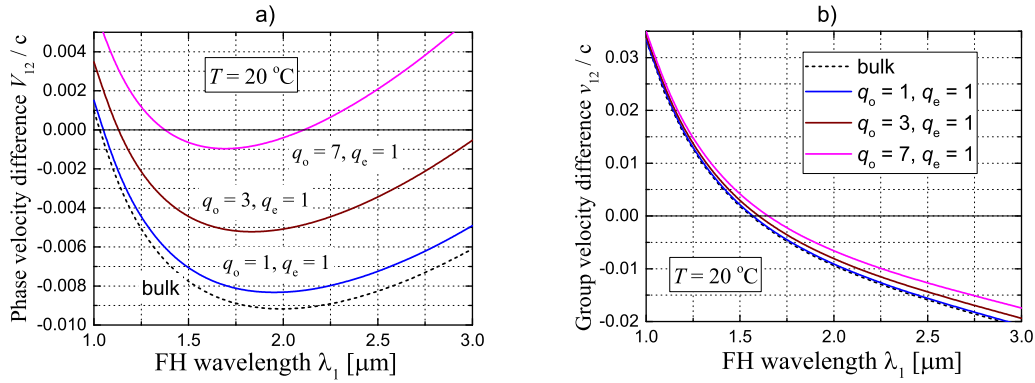walk-off point shifts slowly to the right with increasing q_{o}.

Figure S3. Dependences $V_{12}(\lambda_1)/c$ (a) and $v_{12}(\lambda_1)/c$ (b) for $R = 1$ mm, $r = 0.25$ mm, $T = 20\,^\circ$C, $q_e = 1$, and $q_o = 1, 3$, and 7. The dashed lines correspond to zero geometric dispersion.

Using the above described features of $V_{12}(\lambda_1, T)$ and $v_{12}(\lambda_1, T)$, it is possible to achieve simultaneously a good birefringent phase matching and a small walk-off. To demonstrate this possibility, it is useful to introduce the frequency detuning $\Delta_0 = \omega_2 - 2\omega_1$ instead of V_{12} and the ratio v_{12}/R. Both these parameters have to be normalized to the same modal decay rate γ. Solid lines 1 and 2 in Fig. **??** show λ_1-dependences of these mismatch and walk-off parameters for $q_o = 8$, $q_e = 1$, and $T = 30.4212\,^\circ$C. The dotted line 1' shows what happens with $\Delta_0(\lambda_1)/c$ when the temperature changes to $30.4215\,^\circ$C; it demonstrates a high sensitivity of our adjustment. Within the whole shown range of λ_1, both Δ_0/γ and
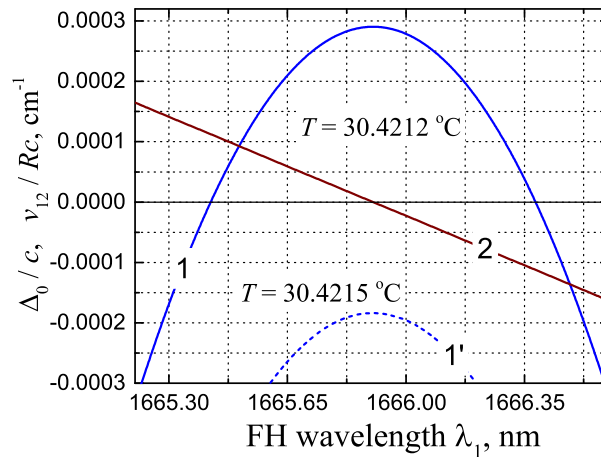

Figure S4. Dependences $\Delta_0(\lambda_1)/c$ (curve 1) and $v_{12}(\lambda_1)/cR$ (curve 2) for $R = 1$ mm, $r = 0.25$ mm, $T = 30.4212\,^\circ$C, $q_o = 8$, and $q_e = 1$. The dashed curve 1' corresponds to $\Delta_0(\lambda_1)/c$ at $T = 30.4215\,^\circ$C; mismatch points are absent here. The corresponding dashed curve for $v_{12}(\lambda_1)/Rc$ practically coincides with curve 2.

$v_{12}/\gamma R$ are $\lesssim 1$ for $\gamma \approx 10^7$ s^{-1}. Note that the wavelength distance between neighboring modes, $\delta\lambda \simeq \lambda^2/2\pi Rn$, is about 0.2 nm for parameters of Fig. **??**, so that several discrete modes are available. It is possible also to make a similar adjustment for $q_o = 7$ (instead of 8). This leads to much higher necessary temperatures, $T \simeq 118.412\,^\circ$C.

3. The effect of radial poling

The quadratic nonlinear optical response of ferroelectric $\chi^{(2)}$ materials, like LiNbO$_3$ or LiTaO$_3$, is determined by the independent real components d_{333} and d_{311} of the third-rank quadratic susceptibility tensor $\hat{d}$ [13]. These components change sign under inversion of the direction of the spontaneous polarization. In the case of perfect radial poling, any of these components (let it be d with the bulk value d_0) changes periodically its sign with the azimuth angle φ, as illustrated by Fig. **??**a for the number of periods $\mathcal{N} = 4$. At the same time, the linear susceptibility tensor and the linear optical properties stay unchanged. If $\mathcal{N}$ is the number of the alternation periods, the function $d(\varphi)$ is $2\pi/\mathcal{N}$-periodic and it can be expanded in the Fourier series, as given by Eq. (6) of the main text. In the case of $\pm$ symmetric domain structure, which is the most suitable for quasi-phase matching, only the Fourier harmonics with numbers $s = \pm\mathcal{N}, \pm3\mathcal{N}, \ldots$ are nonzero.
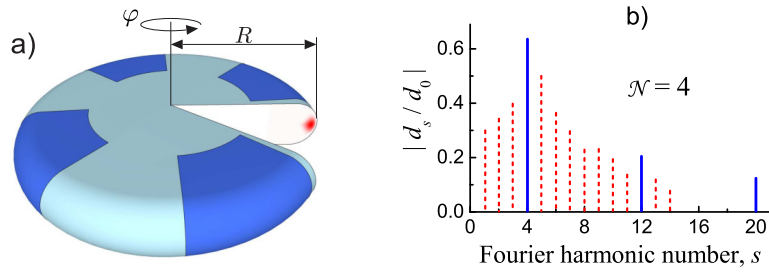
Figure S5. a) Schematic of a periodically poled microresonator of radius R for $\mathcal{N} = 4$. Different colors indicate the radial poling and the red spot indicates localization of light near the rim. b) Blue peaks show the first three harmonics of the corresponding Fourier spectrum with $s = \mathcal{N}, 3\mathcal{N}$, and $5\mathcal{N}$. Red peaks illustrate occurrence of unwanted Fourier harmonics in the case an imperfect radial poling.

For these harmonics, the reduction factor $|d_s/d_0| = 2\mathcal{N}/\pi|s|$ decreases with increasing $|s|$, but remains comparable with 1 for $|s| = \mathcal{N}$, see also Fig. **??**b.

Any disturbance of the $2\pi/\mathcal{N}$ periodicity of the domain structure leads to decrease of the primary Fourier harmonics $d_\mathcal{N}, d_{3\mathcal{N}}, \ldots$ and also to additional Fourier harmonics d_s with $s \neq \mathcal{N}, 3\mathcal{N}, \ldots$ Strong enough distortions can suppress the primary nonlinear phenomena and cause unwanted parasitic nonlinear processes. One of the most dangerous perturbations of the periodicity is off-centering of the radial structure [15]. The well-spread linear poling in commercially available samples of LiNbO$_3$ crystals, is also not suitable for the $\chi^{(2)}$ comb generation.

Consider in some details parameters of the radial poling necessary to achieve the quasi-phase matching near the zero walk-off point $\lambda_2 = \lambda_c \simeq 1.349\,\mu$m for the e-polarized modes. The SH generation conditions in the terms of λ_2 read

$$\frac{n(\lambda_2) - n(2\lambda_2)}{\lambda_2} = \frac{\mathcal{N}}{2\pi R} \equiv \frac{1}{\Lambda}, \tag{4}$$

where Λ is the period of poling of the rim and $n = n_e$. Figure **??** shows dependence $\Lambda(\lambda_2)$ corresponding to this formula.

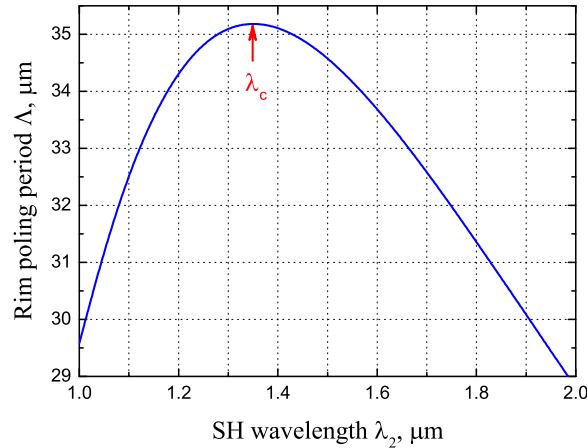**Figure S6.** Rim poling period Λ versus the SH wavelength λ_2. The maximum value $\Lambda_{\max} \simeq 35.2\,\mu$m corresponds to the wavelength $\lambda_c \simeq 1349$ nm.

Remarkably, the maximum value of Λ corresponds with a good accuracy to $\lambda_c \simeq 1.349\,\mu$m. The values of Λ of this scale are accessible for the existing poling techniques. Furthermore, we can estimate $\mathcal{N}$ as 284 for the circumference $2\pi R \simeq 1$ cm.

It is necessary to keep in mind that the above estimates are approximate, for they ignore discreteness of $m_{1,2}$ and $\mathcal{N}$. To get more insights, we represent m_1 and $\mathcal{N}$ as

$$m_1 = \frac{\pi R\, n(2\lambda_2)}{\lambda_2} \quad \text{and} \quad \mathcal{N} = \frac{2\pi R\left[n(\lambda_2) - n(2\lambda_2)\right]}{\lambda_2} \tag{5}$$

and consider dependences $\mathcal{N}(\lambda_2)$ and $m_1(\lambda_2)$ within a 20 nm interval around λ_c. The azimuth number m_1 passes many $(\sim 10^1)$ integer values within this interval and weak variations of R do not matter. The situation with $\mathcal{N}$ is different. In particular, for the circumference $2\pi R = 1$ cm we have $\mathcal{N} \simeq 284.019$ across the whole spectral interval, so that the choice of R is essential to get an integer value of $\mathcal{N}$. In other words, fulfillment of the PM condition at $\lambda_2 \simeq \lambda_c$ can be accomplished only within some narrow windows of R. As $\mathcal{N}$ and m_1 are integers, m_2 is automatically an integer.

In any case, Eqs. (**??**) cannot be satisfied simultaneously without the conventional fine tuning means, such as the temperature or field tuning. With the tuning means, quasi-phase matching becomes possible. By analyzing the effects of fine tuning, it is necessary to keep in mind that when changing the refractive indices $n(\lambda_2)$ and $n(2\lambda_2)$ we shift slightly the zero walk-off point λ_c. Furthermore, employment of fine tuning means can lead to changes of R. Further details are beyond the scope of this section.